Microchimica Acta
https://doi.org/10.1007/s00604-018-3153-3

ORIGINAL PAPER

A fluorometric aptasensor for bisphenol a based on the inner filter effect of gold nanoparticles on the fluorescence of nitrogen-doped carbon dots

Li Wang[1] · Hai-Xia Cao[1] · Chang-Gang Pan[2] · Yu-Sheng He[2] · Hong-Fei Liu[1] · Li-Hong Zhou[1] · Cai-Qi Li[2] · Guo-Xi Liang[2]

Received: 11 September 2018 / Accepted: 7 December 2018

Abstract

An aptamer-based fluorometric assay is described for the determination of bisphenol A (BPA). The aptamer against BPA is first attached to the surface of the red AuNPs, and this prevents the AuNPs from salt-induced formation of a blue-colored aggregate. Hence, the blue fluorescence of added nitrogen-doped carbon dots (NCDots) is quenched via an inner filter effect (IFE) caused by the red AuNPs. After addition of BPA, the BPA/aptamer complex is formed, and the AuNPs are no longer stabilized agains aggregation. This weakens the IFE and results in the recovery of the fluorescence of the NCDots which is measured best at excitation/emission wavelengths of 300/420 nm. The recovered fluorescence increases linearly in the 10 to 250 nM and 250 to 900 nM BPA concentration ranges, and the detection limit is 3.3 nM. The method was successfully applied to the determination of BPA in spiked environmental tap water samples.

Keywords Salt-induced aggregation · Aggregated AuNPs · Fluorescence quenched · Fluorescence recovery · BPA/aptamer complexes · Tap water · Environmental-friendly · Low detection limit · Wide linear range · Quick response

Introduction

Bisphenol A (BPA) is a widely used industrial compound, which has been identified as an endocrine disruptor causing many adverse properties even at very low concentration [1–3]. Considering the adverse properties of BPA, there have been increasing needs for the detection and monitoring of it.

Chromatography [4] and chromatography-mass spectrometry [5] are the most commonly used methods for BPA analysis. They require complex sample pre-treatment, professional operators, expensive equipment, high test charge and considerable time, so they are not suitable for detecting a large number of samples. Therefore, some simple and sensitive alternative assays are developed such as electrochemical [6], immunoassay-based [7] and fluorescent [8] methods. Among these techniques, fluorescent methods have attracted wide attention with the advantages of simplicity, convenient signal transduction, easy operation, and quick response [9].

With the development of nanotechnology, different fluorescence nanomaterials have been reported for applications in fluorescence assays. Carbon dots (CDots) as a class of carbon-based fluorescent nanomaterials possesses interesting properties such as water solubility, biocompatibility, good photostability, and low cytotoxicity. Therefore, CDots have been widely used as ideal fluorescent probes for signal generation and transduction in the fluorescent sensing system [10, 11]. However, because most of the CDots are insensitive or non-selective by recognizing BPA, it is difficult to use them as BPA probes directly [8, 10, 12].

Fluorometric aptasensor based on the inner filter effect (IFE) or fluorescence resonance energy transfer (FRET), on

Electronic supplementary material The online version of this article (https://doi.org/10.1007/s00604-018-3153-3) contains supplementary material, which is available to authorized users.

✉ Li Wang
wangjill@126.com

✉ Guo-Xi Liang
gxliang@ujs.edu.cn

[1] School of Pharmacy, Jiangsu University, Zhenjiang 212013, China

[2] School of the Environment, Jiangsu University, Zhenjiang 212013, China

Published online: 18 December 2018

the other hand, is a solution of this problem. In such strategy, the emission of fluorescer is remarkably inhibited in the presence of dispersed AuNPs via IFE/FRET [13, 14], whereas recovered when AuNPs aggregated. Targets-bound aptamer modulate the aggregation of AuNPs, and then control the IFE/FRET efficiency for signal transfer. So far, this strategy has been used for the detection various analytes including dopamine [15], Hg^{2+} [16], adenosine 5′-triphosphate [17], acetamiprid [18], even BPA [19]. However, to the best of our knowledge, no CDots-based such strategy for BPA detection has been previously reported.

On the other hand, by doping of heteroatoms, the optical and electrical properties of CDots can be improved [20]. A typical doping heteroatom is nitrogen. Therefore, nitrogen-doped CDots (NCDots) can have extensive applications in determination assay based on fluorescence [21–27]. Whereas, compared with synthesis methods, the application research of NCDots is still scarce.

Hence, in the current work, we exploited NCDots as fluorescence indicator to rapidly monitor BPA in an IFE-based aptamer sensing platform. The assay principle is displayed in Scheme 1. The aptasensing system consists of BPA aptamer, AuNPs and NCDots. The dispersive/aggregated AuNPs are acquired through the reaction of the aptamer with BPA. At the absence of BPA, the aptamers coat on the surface of AuNPs to inhibit their aggregation in the high salt solution. In this case, the fluorescent signal of NCDots is quenched by the dispersive AuNPs on the basis of IFE. Upon target BPA introduction, the aptamers bind with the analytes to form new aptamer-BPA complexes, AuNPs tend to be aggregate and the fluorescence of NCDots recovers. This method is relatively environmental-friendly because of the low-toxicity NCDots used. Moreover, BPA can also be easily detected using colorimetric method via color change of AuNPs, and the detection limit can reach 50 nM. In addition, it can be performed at the high salt condition and has a good potential in environmental analysis.

Experimental

Chemicals and materials

BPA is provided by Sigma-Aldrich (St. Louis, MO, USA). L-arginine (L-Arg), ethylenediamine (EDA) and chloroauric acid ($HAuCl_4 \cdot 4H_2O$) are got from Sinopharm Chemical Reagent Co., Ltd. (Shanghai, China) (http://www.sigmaaldrich.biogo.net/). Phenol, Hydroquinone (HQ) and 4, 4′-Dihydroxybiphenyl (BP) are purchased from Aladdin Chemistry Co., Ltd. (Shanghai, China) (http://www.aladdin-e.com/). The anti-BPA aptamer with the sequence of 5′-CCG GTG GGT GGT CAG GTG GGA TAG CGT TCC GCG TAT GGC CCA GCG CAT CAC GGG TTC GCA CCA-3′ is used on the basis the previous studies and synthesized by Sangon Biotechnology Co., Ltd. (Shanghai, China) (http://www.sangon.com/). The anti-BPA aptamer is solved in the ultrapure water with certain volumes for 100 μM of the stocking solution. In the experiment, the aptamer stocking solution is diluted to 200 nM by 0.05 M phosphate buffered solution (pH 7.4) containing 2 mM Mg^{2+}, 10 mM K^+.

All chemicals are of analytical grade without any purification.

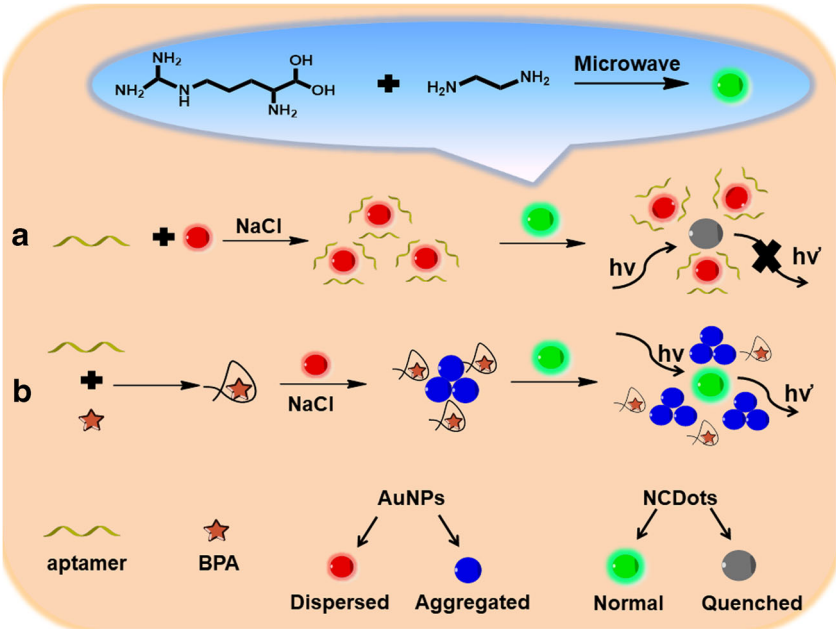

Scheme 1 Schematic presentation of the fluorometric aptasensor for BPA

Instruments

All measurements are carried out under room temperature unless stated. UV-vis spectra are obtained on a UV-2400 UV-VIS-NIR spectrophotometer (Shimadzu) (https://www.shimadzu.com.cn/). The morphology and size of nanoparticles are analyzed using a JEM-2100 transmission electron microscope (HRTEM, JEOL) (http://www.jeol.com.cn/). The fluorescence measurements are carried out on a fluorescence spectrometer (Thermo Scientific Lumina, Thermo) (https://www.thermofisher.com/cn/) with the instrument settings as follows: λ_{ex} = 300 nm (slit 5 nm), λ_{em} = 320–580 nm (slit 5 nm), PMT detector voltage = 600 V. Ultrapure water used throughout the experiment is obtained from the Heal Force water purification system (ROE-100) (http://www.healforce.com/en/).

Synthesis of materials

The NCDots with superior optical properties, outstanding water solubility and low-toxicity are prepared by a microwave-assisted method [28]. The AuNPs synthesized according to the previous report [29] (Electronic Supporting Material, ESM).

Aptamer-based fluorescent detection of BPA

20 μL of 200 nM aptamer solution is mixed with 20 μL BPA solution with different concentrations at 37 °C for 10 min. Afterwards, 500 μL of AuNPs is added and the mixture is incubated at room temperature for 10 min. Next, 100 μL of 15 mM NaCl is added, and incubate for another 10 min. Finally, 100 μL of NCDots solution is added into the above mixture solution, and then gives a final volume of 1 mL with ultrapure water. The fluorescence emission and UV–vis absorption spectra of the resulting solution are recorded immediately.

Determination of BPA in real samples

The tap water samples are taken from our laboratory and filtered using 0.45 μm membrane, then measured according to the method in above Section. For recovery analysis, a certain amount of BPA is added into the samples and analyzes in accordance with the above procedure. Each experiment is repeated three times.

The tap water samples were taken from our laboratory and the urine samples were centrifuged at 12000 g. The tap water samples were taken from our laboratory and the urine samples were got from a health volunteer. Both of them were centrifuged at 12000 g., and then measured according to the method in above Section. For recovery analysis, a certain amount of BPA is added into the samples and analyzes in accordance with the above procedure. Each experiment is repeated three times.

Results and discussions

Characterization of NCDots and AuNPs

NCDots are synthesized according to the microwave assistant method, and exhibit the maximal emission at 420 nm under 300 nm excitation with the fluorescence quantum yield ~0.15 (Fig. S1a). The fluorescence intensity of NCDots did not change remarkably after 1 month. The monodispersed AuNPs are prepared following the classical Frens' citrate reduction route [29], and the maximum UV-vis absorption of the AuNPs is at 523 nm (Fig. S1b). The size, morphology and structure of NCDots and AuNPs are confirmed by transmission electron microscopy (TEM). As shown in Fig. 1, NCDots and AuNPs are all spherical in shape and well dispersed in water, and with average size of ~5 nm and ~13 nm, respectively. XPS of NCDots and IR of NCDots and NCDots/AuNPs are shown in Fig. 2. The NCDots and NCDots/AuNPs have similar IR spectra, suggesting a similar functional groups distribution. To further confirm the functional groups present on the surface of NCDots, XPS characterization was carried out. From the full-scan XPS spectrum of NCDots, C, N, and O are detected with peaks at 286.8 eV (C1s), 400.33 eV (N1 s), and 532.34 eV (O1s) respectively. The XPS spectrum of C1s can be deconvoluted into three surface components corresponding to sp2 (C=C) at 284.5 eV, sp3 (C-C, and C-H) at 285.5 eV, C=O/C=N at 288.3 eV. The surface components of NCDots, as determined by XPS, are in good agreement with the FT-IR results.

Detection principle

This assay is based on the binding of the aptamer with the target can modulate the IFE efficiency of AuNPs on NCDots in NaCl solution as showed in Scheme 1. In the IFE-based fluorescence detection, the overlap between the emission spectrum of fluorescer and the absorption spectrum of absorber is required. Therefore, we firstly verify the spectra overlap. Fig. S1 shows that the emission of NCDots overlaps the absorption spectrum of AuNPs. This demonstrates that IFE can occur. Thus, the effective emission intensity of NCDots is greatly decreased or quenched if NCDots and AuNPs mixed, as shown in Fig. S2.

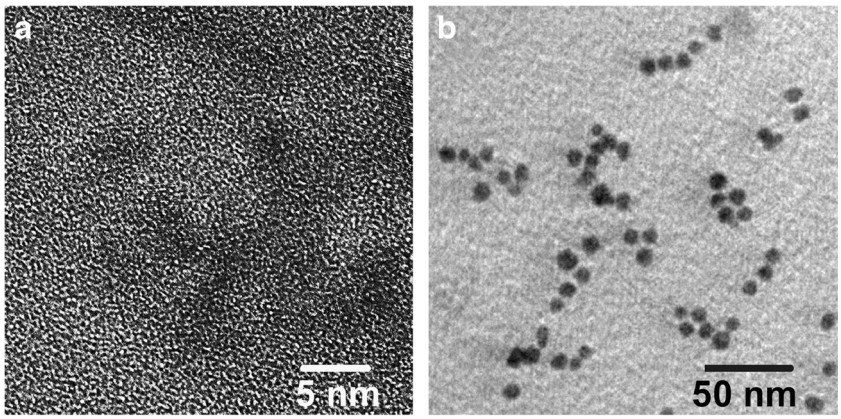

Fig. 1 TEM images of NCDots (**a**) and AuNPs (**b**) dispersed in water

To illustrate the principle for BPA detection, the effects of NaCl, aptamer and BPA-aptamer binding complexes on the fluorescence and absorption spectra of NCDots-AuNPs mixed solution are also investigated in detail.

We firstly investigate the fluorescence spectra of NCDots in each stage, the results are shown in Fig. 3A. Initially, NCDots shows a strong emission peak at 420 nm (Fig 3Aa). When NCDots are mixed with dispersed AuNPs (without NaCl), the emission is significantly quenched via IFE (Fig 3Ab). When ionic strength increases, the charge balance between the AuNPs will be damaged and rapid aggregation occurs [15]. Therefore, the addition of enough salt can screen the repulsion between the nanoparticles, leading to the AuNPs aggregation which provokes a corresponding recovery of IFE-decreased emission of NCDots (Fig 3Ac). The unmodified AuNPs can attach with unfold aptamer and stabilize even in high salt concentration solution and the fluorescence of NCDots decrease again (Fig 3Ad). In contrast, the binding of aptamer with the target can induce AuNPs aggregation in the presence of NaCl [30], and after aggregation the fluorescence of NCDots is greatly enhanced (Fig. 3Ae).

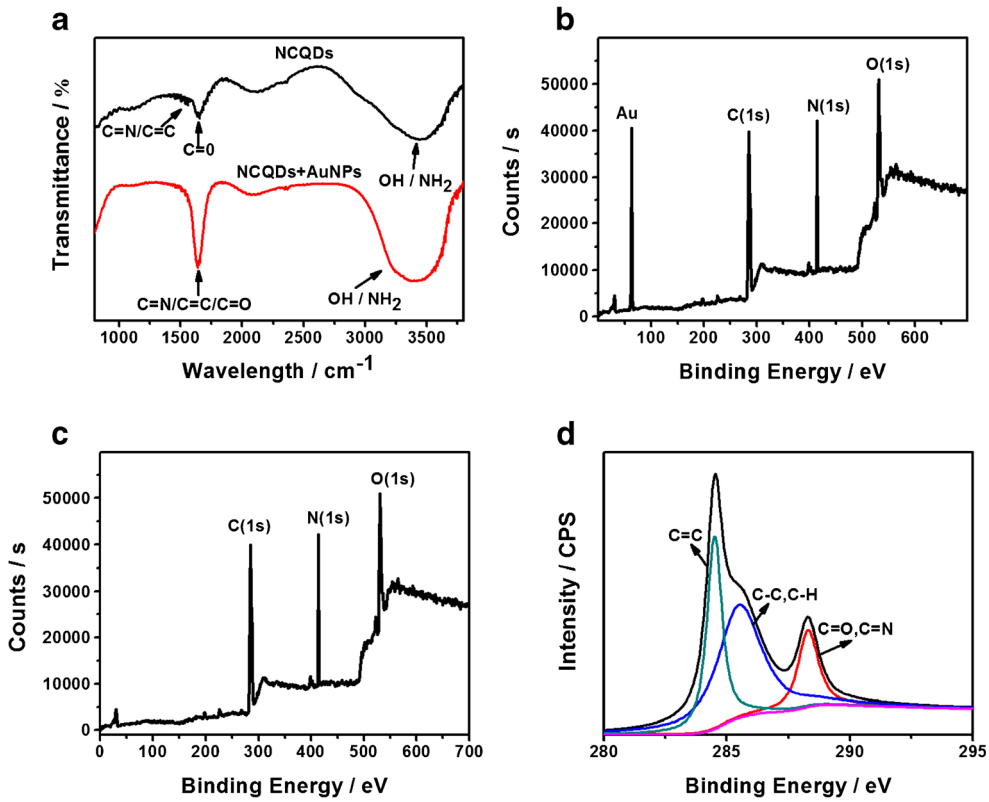

Fig. 2 XPS of NCDots and IR of NCDots and NCDots/AuNPs

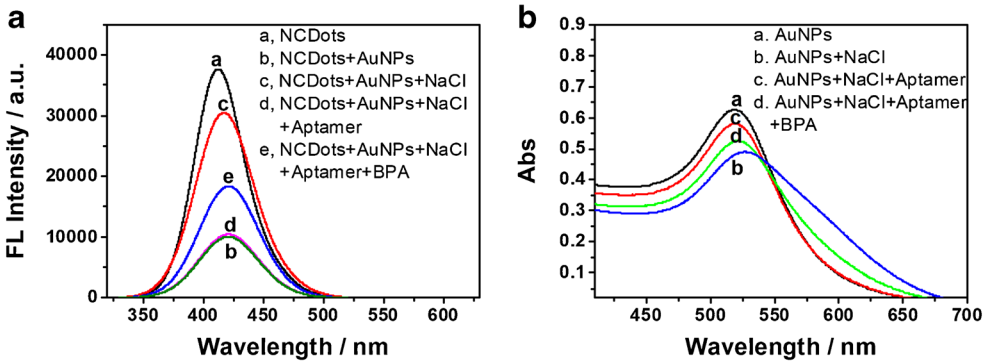

Fig. 3 (A) Fluorescence spectra: **a**, NCDots; **b**, NCDots and AuNPs; **c**, NCDots, AuNPs and NaCl; **d**, NCDots, AuNPs, NaCl and aptamer; **e**, NCDots, AuNPs, NaCl, aptamer and BPA, λex = 300 nm. Insert is the corresponding photographs under UV lamp, λex = 365 nm (B) Absorption spectra: a, AuNPs; b, AuNPs and NaCl; c, AuNPs, NaCl and aptamer; d, AuNPs, NaCl, aptamer and BPA. Aptamer, 250 nM; NaCl, 15 mM; BPA, 250 nM

The corresponding UV-vis absorption spectra of AuNPs in each stage are also recorded in Fig. 3B. Owing to the surface plasmon resonance, the AuNPs dispersed in water solution display an absorption peak at 523 nm (Fig. 3Ba). By adding NaCl, the aggregation of AuNPs occurs, the absorption peak at 523 nm is clearly reduced as shown in Fig. 3Bb. After addition of aptamer, the absorption peak of AuNPs increases, suggesting that aptamer might be absorbed onto the surface of AuNPs and stabilize the AuNPs in salt solution (Fig 3Bc). In the presence of both BPA and aptamer, the absorption intensity is reduced again because the BPA-aptamer complexes cause the aggregate of AuNPs (Fig 3Bd).

To clearly verify such aggregation and disperse of the AuNPs, the corresponding TEM images are also collected (Fig. 4). As indicated, initially, AuNPs are dispersed in aqueous solution (Fig. 4a). In addition of NaCl, AuNPs aggregate (Fig. 4b). Afterward, the aggregation of AuNPs becomes dispersed upon addition of aptamer (Fig. 4c). Finally, when the mixture of BPA and aptamer is added, the AuNPs is aggregated again (Fig. 4d). Because the amount of NCDots is much smaller than AuNPs, it is different to observe their TEM images. Therefore, we only observe the AuNPs TEM images at different conditions.

The fluorescence, absorption spectra and TEM image results are all consistent with the mechanism illustrated in Scheme 1.

Optimization of the experimental conditions

On the purpose of acquiring the satisfactory detection efficiency of the method, the significant factors affected the response of the experiment were optimized.

The concentration of salt played an important role in AuNPs aggregation as discussed above. Therefore, we firstly investigate the effect of concentration of NaCl on the assay by monitoring the fluorescence change. It is seen that with the increase of NaCl concentration, the fluorescence signal increases gradually until to 15 mM (Fig. S3A). 15 mM NaCl is selected for further experiment.

The following parameters are also optimized by monitoring the fluorescence of the assay system under different conditions: concentration of aptamer, reaction temperature and time, AuNPs amount. The optimum concentration of aptamer is chosen to be 200 nM (Fig. S3B). The best binding temperature and time of BPA with aptamer are 37 °C and 10 min, respectively (Fig. S3C and D). The optimum AuNPs amount is chosen to be 500 μL (Fig. S4).

Sensitivity and selectivity

As the assay principle described above, BPA can increase the fluorescence intensity of NCDots in the system. Under the optimum conditions, the enhanced intensity is in proportion to the concentration of BPA (Fig. 5a). Insert shows the corresponding fluorescence color change with the amount of BPA ranging from 10 to 900 nM (from right to left: concentrations of BPA were 10 nM, 40 nM, 80 nM, 100 nM, 120 nM, 250 nM, 400 nM, 600 nM, 750 nM, 900 nM, respectively). The concentrations of BPA are ranged from 10 to 900 nM, we obtain two linear regression equations: $I = 33.131c + 10{,}521$ ($r = 0.9984$, 10–250 nM) and $I = 22.5\ c + 13{,}378$ ($r = 0.9989$, 250–900 nM), and a detection limit of 3.3 nM is calculated using the 3σ rule ($\sigma = S_0/S$, S_0 is known as the standard deviation of the

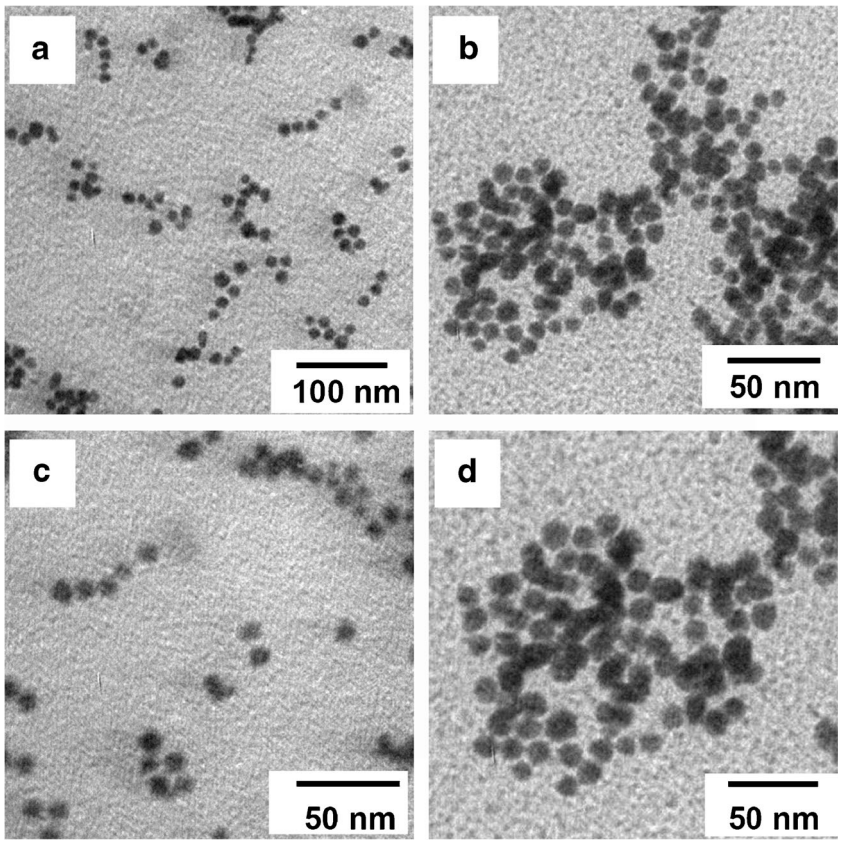

Fig. 4 TEM images of AuNPs in different systems. **a** AuNPs; **b** AuNPs+NaCl; **c** AuNPs+NaCl+ aptamer; **d** AuNPs+NaCl+ aptamer+BPA. Aptamer, 250 nM; NaCl, 15 mM; BPA, 125 nM

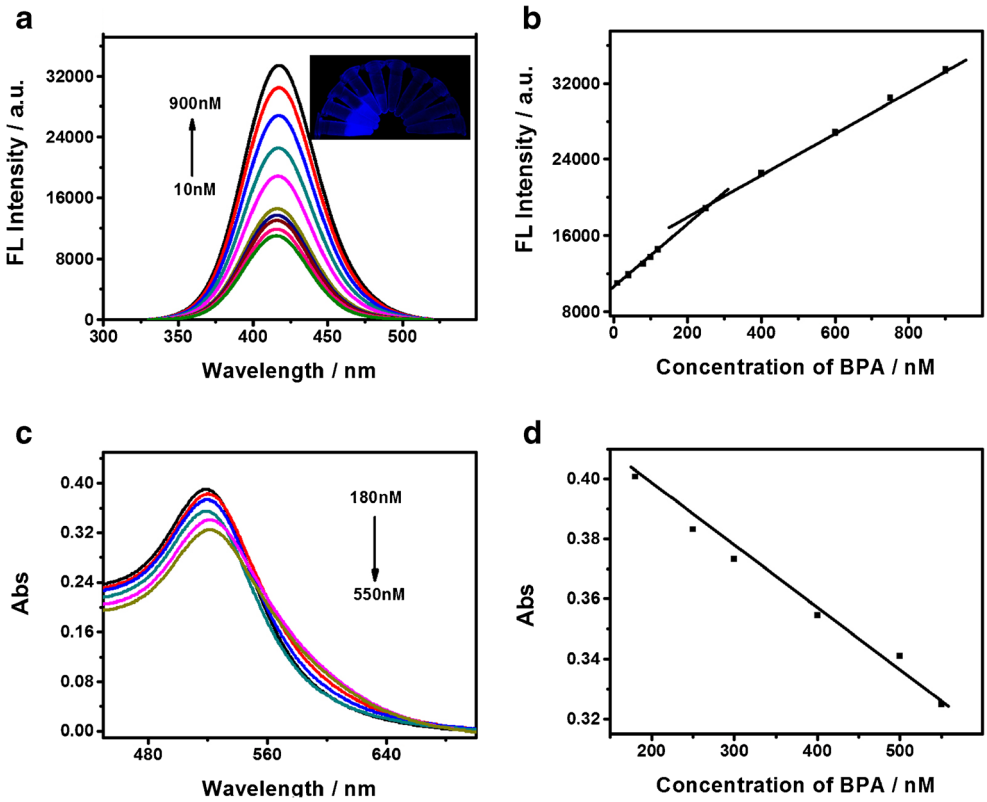

Fig 5 **a**, **c** Fluorescence, absorption spectra of the detection system with the increasing concentrations of BPA, λex = 300 nm. **b**, **d** The corresponding linear calibration plots. NaCl, 15 mM; aptamer, 250 nM. (λex = 300 nm, λem = 420 nm, λAbs = 523 nm)

blank after repeated measurements, and S is the slope of the calibration plot) (Fig. 5b). Correspondingly, as shown in Fig. 5c and d, the UV-vis absorbance intensity of AuNPs reduced gradually with increasing concentrations of BPA and shown good linear relationship ranging from 180 nM to 550 nM with a LOD of 50 nM. Based on fluorescent and colorimetric dual mode detection, we can more accurately and intuitively detect BPA.

Compared with most other previously published strategies for BPA detection (Table 1), the method here is capable of offering higher detection sensitivity and selectivity, with less cost and lower environmental toxicity.

The selectivity of the method was investigated by observing potential interferences of other molecules such as analogues (phenol, hydroquinone, 4,4′-dihydroxybiphenyl, bisphenol S, bisphenol F, o-nitrophenol, paranitrophenol), and some ions (Fe^{3+}, Fe^{2+}, Cu^{2+}, Cu^{+}, Hg^{2+}, Ca^{2+}, Ba^{2+}, S^{2-}, NO_3^-, Pb^{2+}, Hg^{2+} and Ag^{+}). As clearly shown in Fig. 6, these competitors did not interfere with the results of the proposed method.

Application to real samples

To evaluate this method in real samples, the assay is used to determine BPA in tap water. The fluorescence results demonstrate that all samples do not contain any detectable amount of BPA. Then, different concentrations of BPA standard solutions are added in the samples to perform the recovery experiments. The spiked samples are directly analyzed according to the fluorescence assay procedures described above without any further pretreatments. As summarized in Table 2, the recovery varies from 95% to 101% with relative standard deviation values of <1.2%, indicating that this method is highly reproducible and accurate for routine analysis of BPA in tap water samples. In addition, the acquired results were verified with a HPLC method.

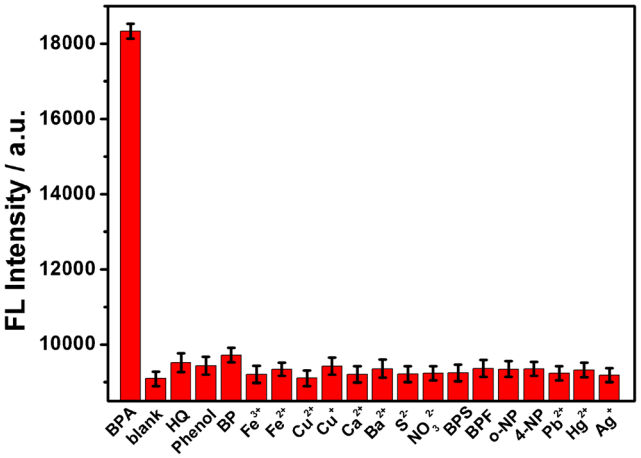

Fig. 6 The specificity of our method against some potential interferences hydroquinone (HQ), phenol, 4,4′-dihydroxybiphenyl (BP), bisphenol S (BPS), bisphenol F (BPS), o-nitrophenol (o-NP), Paranitrophenol (4-NP), Fe^{3+}, Fe^{2+}, Cu^{2+}, Cu^{+}, Ca^{2+}, Ba^{2+}, S^{2-}, NO_3^-, Pb^{2+}, Hg^{2+} and Ag^{+}. The concentration of BPA is 250 nM and the others are the same concentration. Each data point represents the average value of three independent experiments with error bars

Conclusions

To summarize, a novel method for detecting BPA is proposed based on the specific recognition of aptamer and the IFE of AuNPs on the fluorescence of NCDots. This strategy possesses several advantages: Firstly, the method is environmental-friendly and cost efficiency since NCDots is low toxic and inexpensive. Secondly, it is a quick and convenient detection because both signal probe and aptamer do not need labeling or modifying. Thirdly, the assay can greatly shorten the time required for analysis by avoiding the separation and washing steps. The whole detection process can be completed in 35 min. In addition, through merely replacing the corresponding aptamer, this method can be further utilized to analyze a wide range of small molecules. The main limitation for the application of this method in analysis may be the interference from fluorescence species emitting on the ultraviolet-visible range. Further attention may be focused on the development of near infrared (NIR) emitting CDots-based aptasensor.

Table 1 Comparison of linear range and LOD of different fluorescence methods for detection of BPA. (MIP: molecularly imprinted polymers; MGO: magnetic oxidation graphene)

Method	System	LOD	Linear range	References
Fluorescence	MIP-coated CDots	30 nM	100–4200 nM	[12]
Fluorescence	CdTe QDs/AuNPs/NaCl/aptamer	1.86 ng/mL	10–80 ng/mL	[13]
Fluorescence	labeled BPA aptamer/MGO	0.071 ng/mL	0.2–10 ng/mL	[31]
Fluorescence	MIP-coated AgNCs	0.02 μg/mL	0.2 μg/mL-2 mg/L	[32]
Fluorescence	NCDots/AuNPs/NaCl/aptamer	3.3 nM	10–900 nM	This work

Table 2 Application of this method for the determination of BPA in tap water and urine samples spiked with different amounts of BPA ($n = 3$)

Samples	Found (nM)	Spiked (nM) [a]	Determinded (nM)		Recovery (%)		RSD (%)	
			This work	HPLC[b]	This work	HPLC	This work	HPLC
Tap Water	–	80	78	82	97.5	102.5	1.21	1.11
		100	99	104	99.0	104.0	1.98	1.68
		250	252	256	100.8	102.4	1.91	1.28
Urine	–	80	76	84	95.0	105.0	1.56	1.23
		100	101	106	101.0	106.0	1.95	1.24
		250	249	254	99.6	101.6	1.67	1.18

a the final concentration in sample

b method are described in detail in Electronic Supporting Material

Acknowledgements This work was financially supported by National Natural Science Foundation of China (No. 21707053), Natural Science Foundation of Jiangsu Province (No. BK20140577), and Advanced Talents Science Foundation of Jiangsu University (No. 10JDG052, 10JDG038).

Compliance with ethical standards The author(s) declare that they have no competing interests.

References

1. Rochester JR (2013) Bisphenol a and human health: a review of the literature. Reprod Toxicol 42:132–155
2. Vogel SA (2009) The politics of plastics: the making and unmaking of bisphenol a safety. Am J Public Health 99:S559–S566
3. Guida M, Troisi J, Ciccone C, Granozio G, Cosimato C, Di Spiezio Sardo A, Ferrara C, Guida M, Nappi C, Zullo F, Di Carlo C (2014) Bisphenol a and congenital developmental defects in humans. Mutat Res 774:33–39
4. Sungur S, Koroglu M, Ozkan A (2014) Determinatıon of bisphenol a migrating from canned food and beverages in markets. Food Chem 142:87–91
5. Jiao Y, Ding L, Fu S, Zhu S, Li H, Wang L (2012) Determination of bisphenol a, bisphenol F and their diglycidyl ethers in environmental water by solid phase extraction using magnetic multiwalled carbon nanotubes followed by GC-MS/MS. Anal Methods 4:291–298
6. Güney S, Güney O (2017) Development of an electrochemical sensor based on covalent molecular imprinting for selective determination of bisphenol-a. Electroanal 29:2579–2590
7. Miao W, Wei B, Yang R, Wu C, Lou D, Jiang W, Zhou Z (2014) Highly specific and sensitive detection of bisphenol a in water samples using an enzyme-linked immunosorbent assay employing a novel synthetic antigen. New J Chem 38:669–675
8. Wu Y, Liu Y, Gao X, Gao K, Xia H, Luo M, Wang X, Ye L, Shi Y, Lu B (2015) Monitoring bisphenol a and its biodegradation in water using a fluorescent molecularly imprinted chemosensor. Chemosphere 119:515–523
9. Zhong W (2009) Nanomaterials in fluorescence-based biosensing. Anal Bioanal Chem 394:47–59
10. Xiang GQ, Ren Y, Xia Y, Mao W, Fan C, Guo SY, Wang PP, Yang DH, He L, Jiang X (2017) Carbon-dot-based dual-emission silica nanoparticles as a ratiometric fluorescent probe for bisphenol a. Spectrochim Acta A 177:153–157
11. Miaomiao Z, Huixiang J, Li Z, Mingzhong S, Zhongwei Z, Zhenyu D, Lirong Z, Aihua G, Chaoyao W, Fengyi D (2015) Engineering iodine-doped carbon dots as dual-modal probes for fluorescence and X-ray CT imaging. Int J Nanomedicine 10:6943–6953
12. Liu GL, Chen Z, Jiang XY, Feng DQ, Zhao JY, Fan DH, Wang W (2016) In-situ hydrothermal synthesis of molecularly imprinted polymers coated carbon dots for fluorescent detection of bisphenol a. Sens Actuators B Chem 228:302–307
13. Cui X, Liu M, Li B (2012) Homogeneous fluorescence-based immunoassay via inner filter effect of gold nanoparticles on fluorescence of CdTe quantum dots. Analyst 137:3293–3299
14. Wang JL, Wu YG, Zhou P, Yang WP, Tao H (2018) A novel fluorescent aptasensor for ultrasensitive and selective detection of acetamiprid pesticide based on inner filter effect between gold nanoparticles and carbon dots. Analyst 143:5151–5160
15. Xu J, Li Y, Wang L, Huang Y, Liu D, Sun R, Luo J, Sun C (2015) A facile aptamer-based sensing strategy for dopamine through the fluorescence resonance energy transfer between rhodamine B and gold nanoparticles Author links open overlay panel. Dyes Pigments 123:55–63
16. Yu T, Zhang T-T, Zhao W, Xu J-J, Chen H-Y (2017) A colorimetric/fluorescent dual-mode sensor for ultra-sensitive detection of Hg^{2+}. Talanta 165:570–576
17. Xu M, Gao Z, Zhou Q, Lin Y, Lu M, Tang D (2016) Terbium ion-coordinated carbon dots for fluorescent aptasensing of adenosine 5′-triphosphate with unmodified gold nanoparticles. Biosens Bioelectron 86:978–984
18. Guo J, Li Y, Wang L, Xu J, Huang Y, Luo Y, Shen F, Sun C, Meng R (2016) Aptamer-based fluorescent screening assay for acetamiprid via inner filter effect of gold nanoparticles on the fluorescence of CdTe quantum dots. Anal Bioanal Chem 408:557–566
19. Li Y, Xu J, Wang L, Huang Y, Guo J, Cao X, Shen F, Luo Y, Sun C (2016) Aptamer-based fluorescent detection of bisphenol a using nonconjugated gold nanoparticles and CdTe quantum dots. Sens Actuators B Chem 222:815–822
20. Zhu S, Meng Q, Wang L, Zhang J, Song Y, Jin H, Zhang K, Sun H, Wang H, Yang B (2013) Highly photoluminescent carbon dots for multicolor patterning, sensors, and bioimaging. Angew Chem 52(14):3953–3957
21. Wang Y, Yang Y, Liu W, Ding F, Zhao Q, Zou P, Wang X, Rao H (2018) Colorimetric and fluorometric determination of uric acid based on the use of nitrogen-doped carbon quantum dots and silver triangular nanoprisms. Microchim Acta 185:281–289
22. Li D, Nie F, Tang T, Tian K (2018) Determination of ferric ion via its effect on the enhancement of the chemiluminescece of the

permanganate-sulfite system by nitrogen-doped graphene quantum dots. Microchim Acta 185:431–438
23. Atchudan R, Tnji E, Aseer KR, Perumal S, Karthik N, Lee YR (2017) Highly fluorescent nitrogen-doped carbon dots derived from Phyllanthus acidus utilized as a fluorescent probe for label-free selective detection of Fe^{3+} ions, live cell imaging and fluorescent ink. Biosens Bioelectron 99:303–311
24. Iqbal A, Iqbal K, Xu L, Li B, Gong D, Liu X, Guo Y, Liu W, Qin W, Guo H (2018) Heterogeneous synthesis of nitrogen-doped carbon dots prepared via anhydrous citric acid and melamine for selective and sensitive turn on-off-on detection of hg (II), glutathione and its cellular imaging. Sensors Actuators B Chem 255:1130–1138
25. Huang Q, Li Q, Chen Y, Tong L, Lin X, Zhu J, Tong Q (2018) High quantum yield nitrogen-doped carbon dots: green synthesis and application as "off-on" fluorescent sensors for the determination of Fe^{3+} and adenosine triphosphate in biological samples. Sensors Actuators B Chem 276:82–88
26. Walekar LS, Hu P, Liao F, Guo X, Long M (2018) Turn-on fluorometric and colorimetric probe for hydrogen peroxide based on the in-situ formation of silver ions from a composite made from N-doped carbon quantum dots and silver nanoparticles. Microchim Acta 185:31–39
27. Gomez IJ, Arnaiz B, Cacioppo M, Arcudi F, Prato M (2018) Nitrogen-doped carbon Nanodots for bioimaging and delivery of paclitaxel. J Mater Chem B 6:5540–5548
28. Arcudi F, Đorđević L, Prato M (2016) Synthesis, separation, and characterization of small and highly fluorescent nitrogen-doped carbon nanodots. Angew Chem Int Ed 55:2107–2112
29. Frens G (1973) Controlled nucleation for the regulation of the particle size in monodisperse gold suspensions. Nat Phys Sci 241:20–22
30. Qi Y, Li B (2011) A sensitive, label-free, aptamer-based biosensor using a gold nanoparticle-initiated chemiluminescence system. Chem-Eur J 17:1642–1648
31. Hu LY, Niu CG, Wang XY, Huang DW, Zhang L, Zeng GM (2017) Magnetic separate "turn-on" fluorescent biosensor for bisphenol a based on magnetic oxidation graphene. Talanta 168:196–202
32. Deng C, Zhong Y, He Y, Ge Y, Song G (2016) Selective determination of trace bisphenol a using molecularly imprinted silica nanoparticles containing quenchable fluorescent silver nanoclusters. Microchim Acta 183:431–439